A Method to Design Power Control System of Wayside Energy Storage System for Energy Saving in DC-electrified Railway

Kota Sato*, Keiichiro Kondo*, Hiroyasu Kobayashi**, Makoto Chida***
* Department of Electrical Engineering and Bioscience, Waseda University, Tokyo, Japan
**Department of Electrical and Electronic Engineering, Chiba University, Chiba, Japan
*** Innovation Department, West Japan Railway Company, Osaka, Japan
Tel.: +813 –5286 – 3184.
E-Mail: sugarballs@fuji.waseda.jp
URL: http://www.kondolab.eb.waseda.ac.jp/access/

Keywords

«Railway traction system», «DC railway power supply», «Energy storage», «Battery», «Regenerative power»

Abstract

The energy-saving effect of the use of a wayside energy storage system (WESS) power control method is improved by increasing the controller gain of the WESS for DC-electrified railways. However, excessive gain may cause instability. Therefore, this study proposes a method for designing a charge/discharge current controller.

1. Introduction

Regenerative braking enables to recover the kinetic energy at deceleration electrical energy and increase the energy efficiency of electric railways [1]. However, because DC-electrified railway systems generally use diode rectifiers at substations, regenerative energy cannot be returned to the AC grid. Thus, only a fraction of the regenerative energy is effectively used if powering trains absorbed all of the regenerative energy. One of the solutions to the problem of regenerative energy is installation of energy storage systems to utilize the excess regenerative energy. There are two types of energy storage systems: onboard energy storage systems [2] and wayside energy storage systems (WESSs) [3][4]. Onboard energy storage system can more efficiently utilize regenerative energy on the vehicle and is also effective for emergency power supply [5][6]. However, the amount of onboard batteries is greatly affected by the space and weight constraints of the railway vehicle. On the other hand, WESS, as shown in Fig.1, is more advantageous to avoid to increase the mass of the train and is more cost effective for the energy saving by recovering the waste regenerative energy. In the WESS, batteries are connected by bi-directional non-isolated DC/DC converter [7] to catenary line to boost up its voltage and for charge and discharge control. The charge and discharge control of the WESS is carried out by the current control based on the voltage at the overhead catenary line connection point, as shown in Fig. 2. The energy saving effect is improved by increasing the gain K_{ref}. However, if the gain K_{ref} becomes too high, the

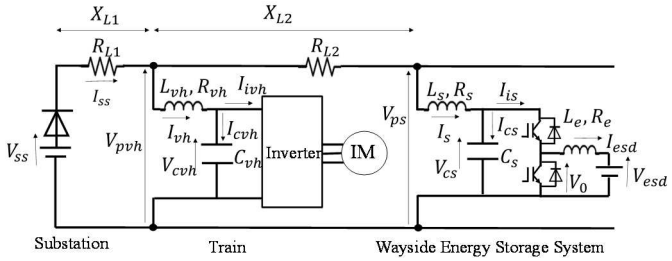

Fig. 1. WESS model with a powering train and a substation

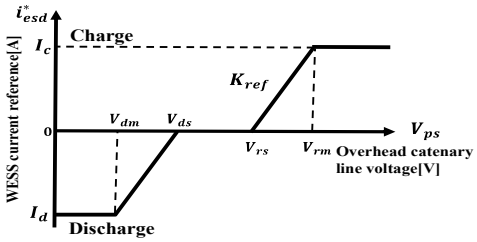

Fig. 2. Determination pattern of WESS current reference

phase margin of the control system decreases, which leads to unstable phenomena such as sustained oscillation or divergence [8].

Several methods have been proposed to suppress the oscillation of the system by connecting voltage-type power converters to a common DC link, similar to DC-electrified railway systems, utilizing the additional circuits [9]. However, in DC-electrified railways system, additional equipment is not desirable because of its higher cost. Another method involves the use of a control system model that suppresses oscillation by controlling the bidirectional power converter on the power-supply side [10] [11]. However, stabilization by controlling the power-supply side is impossible for DC-electrified railway systems because the diode rectifier is utilized as the power converter of the power supply substation, as previously mentioned. The value of the inductance of the filter reactor (FL) in a DC-electrified railway system is set to a large value to prevent the increase of the short-circuit current in the event of an accident. Therefore, when the discharge current on the low-voltage side of the WESS increases significantly, the current of the FL does not; hence, the current of the filter capacitor (FC) increases, while the FC voltage becomes large and oscillatory, leading to the instability phenomena.

Therefore, it is necessary to design the power control system of the WESS to maintain stability. However, a method for determining the gain K_{ref}, which causes instability, has not been established. In this study, a linearized model of a DC feeder circuit which includes WESS, is derived. Then, a design method for the WESS power control system based on the derived model is proposed to enhance the energy efficiency of the DC-electrified railway system. In the proposed linearization model, two patterns of the assumed circuit configurations are considered: (i) when the train is powering and the WESS is discharging, and (ii) when the train is regenerating and the WESS is charging. The proposed design method was verified experimentally utilizing a downscaled model. In addition, the energy efficiency of the proposed design method was investigated by the numerical simulation of a real-scaled DC-electrified railway system with a WESS. By establishing a method to determine the gain K_{ref}, it is possible to realize charge/discharge control with a high energy efficiency while maintaining the stability of the WESS.

2. Modeling and designing the WESS charge/discharge control system

In this section, a linearized model is derived for the charge/discharge power control system of a WESS. Based on this, the design method of the charge/discharge power control system using Bode diagrams is explained.

A. Modeling the power feeding system and the controller for WESS

In this section, a linearized model of the assumed system, as shown in Fig.1, is described. The two patterns described above are considered as the assumed system. In case (i), the overhead catenary line voltage of the train is lower than the voltage at the substation, and diodes of the substation are turned on. The circuit configuration that includes a substation is assumed. In case (ii), the overhead catenary

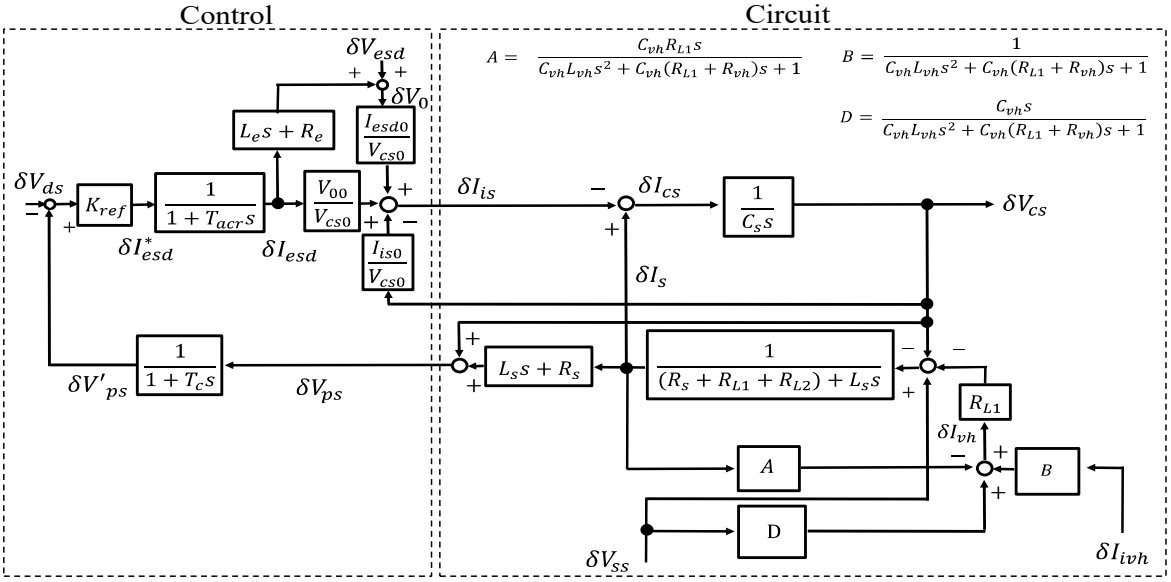

Fig. 3. A linearized model including powering-train, WESS, and substation

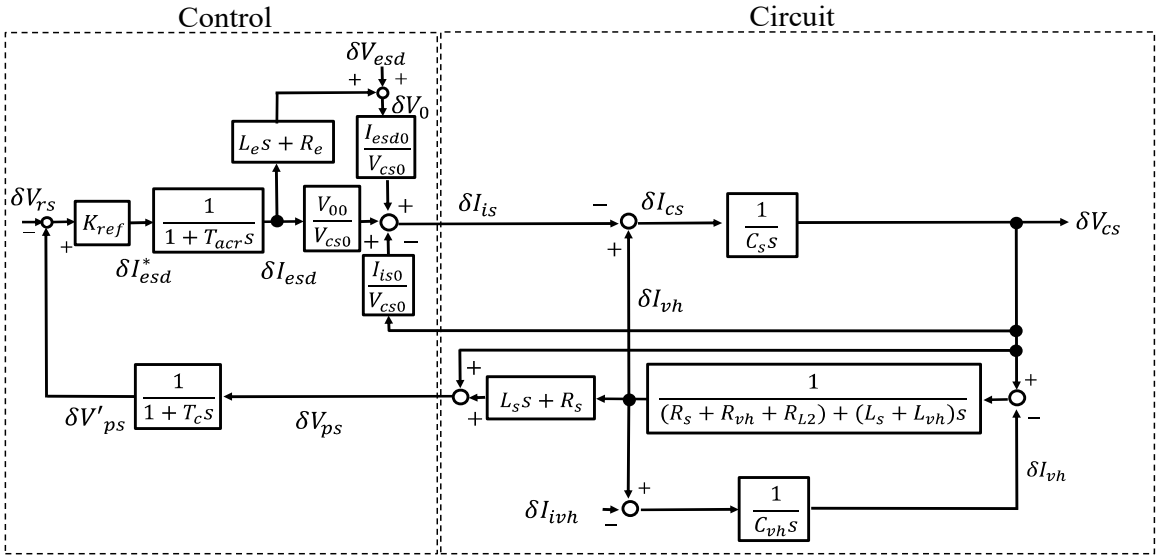

Fig. 4. A linearized model including regenerative train and WESS

line voltage of the train is higher than the voltage at the substation, and diodes of the substation are turned off. Therefore, a circuit configuration consisting of only a train and a WESS is assumed (Fig. 1). The control system and circuit equations in case (i) are explained.

The charge/discharge current I_{esd} of the WESS corresponds to the reference current I^*_{esd} with a first-order delay, and equation (1) holds.

$$I_{\mathrm{esd}} = \frac{1}{1+T_{\mathrm{acr}}s} I^*_{\mathrm{esd}} \tag{1}$$

For the two-quadrant chopper of the WESS, equation (2) holds, assuming that there are ~~zero~~ no losses in the power conversion.

$$V_{\mathrm{cs}} \cdot I_{\mathrm{is}} = V_0 \cdot I_{\mathrm{esd}} \tag{2}$$

Equation (2) is a nonlinear equation; therefore, considering the small variation near the equilibrium point, it is linearized by equation (3) from the Taylor expansion. In equation (3), "0" represents the equilibrium point, and "δ" represents the small variation from the equilibrium point.

$$\delta I_{\mathrm{is}} = \frac{V_{0(0)}}{V_{\mathrm{cs}(0)}} \cdot \delta I_{esd} + \frac{I_{\mathrm{esd}(0)}}{V_{\mathrm{cs}(0)}} \cdot \delta V_0 - \frac{I_{\mathrm{is}(0)}}{V_{\mathrm{cs}(0)}} \cdot \delta V_{\mathrm{cs}} \tag{3}$$

As equation (3) is a nonlinear equation, it can be expressed as a linear equation by the Taylor expansion around the equilibrium point.

The lower side voltage of the chopper V_0 is expressed by equation (4).

$$V_0 = V_{\mathrm{esd}} - (R_{\mathrm{e}} I_{\mathrm{esd}} + L_{\mathrm{e}} \frac{d}{dt} I_{\mathrm{esd}}) \tag{4}$$

Equation (5) shows the relationship between the current and voltage of the DC-link capacitor of the WESS.

$$C_{\mathrm{s}} \frac{d}{dt} V_{\mathrm{cs}} = I_{\mathrm{s}} - I_{\mathrm{is}} \tag{5}$$

The overhead catenary line voltage of the WESS V_{ps} is expressed by equation (6).

$$V_{\mathrm{ps}} = V_{\mathrm{cs}} + (R_{\mathrm{s}} I_s + L_s \frac{d}{dt} I_s) \tag{6}$$

Equation (7) holds for the DC-link voltage of the train V_{cvh}.

$$V_{\mathrm{cvh}} = V_{\mathrm{ss}} - R_{\mathrm{L1}} I_{\mathrm{vh}} - \left\{ (R_{\mathrm{s}} + R_{\mathrm{L1}} + R_{L2}) I_s + L_s \frac{d}{dt} I_s \right\} \tag{7}$$

Equation (8) shows the relationship between the current and voltage of the DC-link capacitor of the train.

$$C_{\mathrm{vh}} \frac{d}{dt} V_{\mathrm{cvh}} = I_{\mathrm{vh}} - I_{\mathrm{ivh}} \tag{8}$$

The voltage source inverter with constant current control on the AC side can be regarded as the current source from the DC side. Therefore, the train model consists of the FL, FC, and current source.
Next, the circuit equations for case (ii) are shown. In case (ii), equations (1) – (6) and (8) are the same as those in case (i); only equation (7) is different. As previously mentioned, diodes of the substation are turned off; hence, the circuit configuration in case (i) consists of the train and the WESS. Therefore, the train current I_{vh} is expressed by equation (9).

$$I_{\mathrm{vh}} = -I_{\mathrm{s}} \tag{9}$$

The voltage equation that includes the train DC-link voltage and the WESS DC-link voltage is expressed by equation (10).

$$V_{\mathrm{cs}} = (R_{\mathrm{s}} + R_{\mathrm{vh}} + R_{\mathrm{L2}})I_{\mathrm{vh}} + (L_{\mathrm{s}} + L_{\mathrm{vh}})\frac{d}{dt}I_{\mathrm{vh}} + V_{\mathrm{cvh}} \tag{10}$$

The block diagrams for case (i) and (ii) are shown in Fig. 3 and Fig. 4, respectively.

B. *Calculation of theoretical stability limits*

The open-loop transfer function from the discharge start voltage δV_{ds} to the overhead catenary line voltage $\delta V'_{\mathrm{ps}}$ in Fig. 3 is shown on the Bode diagram. The open-loop transfer function from the charge start voltage δV_{rs} to the overhead catenary line voltage $\delta V'_{\mathrm{ps}}$ in Fig. 4 is also shown on the Bode diagram. From the phase margin, the stability limit gain K_{ref} is obtained. The parameters in Table I are obtained based on the parameters of the 1 kW class downscaled experimental system described in Section 3. The value of the feeder resistance R_{L1} is determined based on the case of $X_{\mathrm{L1}} = 4$. The value of R_{L1} is set to 12.5 Ω to match the rate of voltage

Table I. Parameters of the assumed system

Symbol	Parameters	Value
C_{vh}	FC capacitance of the train	1320 μF
L_{vh}	FL inductance of the train	80 mH
R_{vh}	FL resistance of the train	0.7 Ω
C_s	FC capacitance of the wayside energy storage system	1320 μF
L_s	FL inductance of the wayside energy storage system	80 mH
R_s	FL resistance of the wayside energy storage system	0.7 Ω
X_{L1}	Distance between the train and the wayside energy storage system	4 km
X_{L2}	Distance between the train and substation	4 km
R_{L1}	Feeder resistance between the train and the wayside energy storage system	12.5 Ω
R_{L2}	Feeder resistance between the train and substation	12.5 Ω
L_e	WESS Low voltage side FL inductance	20 mH
R_e	WESS low voltage side FL resistance	0.25 Ω
T_{acr}	Time constant of current control	5 ms
T_c	Time constant of low-pass filter	50 ms

Table II. Equilibrium points and phase margin at each gain in case (i)

(a) Equilibrium points in case (i)

Parameters	K_{ref} = 1	K_{ref} = 2	K_{ref} = 3	K_{ref} = 4	K_{ref} = 5
Chopper inflow current I_{is0} [A]	3.88	3.84	3.83	3.83	3.82
WESS FC voltage V_{cs0}[V]	295.9	300.5	302.3	303.3	303.9
Chopper lower side voltage V_{00}[V]	49.4	49.1	49.0	48.9	48.8
Discharge current I_{esd0}[A]	10.4	11.6	12.1	12.3	12.5

(b) Phase margin in case (i)

Gain value	Phase margin[deg]
1	+45
2	+28
3	+15
4	+4
5	-5

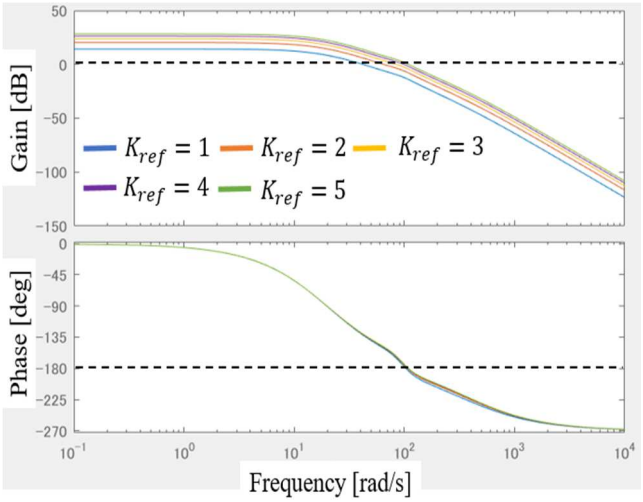

Fig. 5. Bode diagram of the open-loop transfer function from V_{ds} to V'_{ps} in case (i) (K_{ref} = 1, 2, 3,4, 5)

Table III. Equilibrium points and Phase margin at each gain in case (ii)

(a) Equilibrium points in case (ii)

Parameters	K_{ref} = 1	K_{ref} = 2	K_{ref} = 3	K_{ref} = 4	K_{ref} = 5
Chopper inflow current I_{is0} [A]	1.50	1.51	1.52	1.52	1.53
WESS FC voltage V_{cs0}[V]	313.6	309.3	307.8	307.1	306.7
Chopper lower side voltage V_{00}[V]	54.1	54.2	54.2	54.2	54.2
Discharge current I_{esd0}[A]	8.66	8.64	8.63	8.63	8.62

(b) Phase margin in case (ii)

Gain value	Phase margin[deg]
1	+36
2	+25
3	+10
4	-1
5	-9

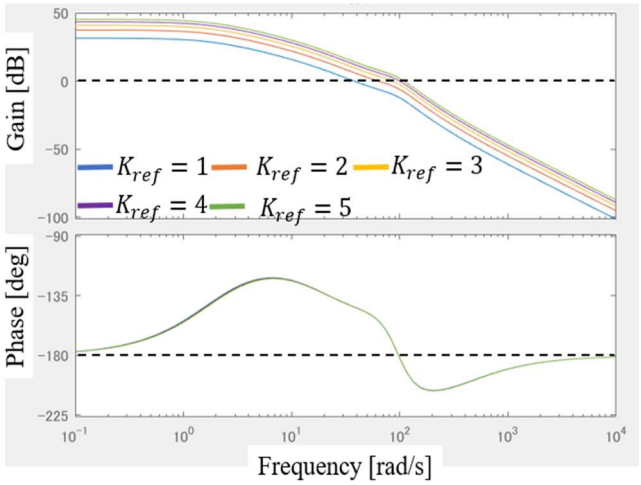

Fig. 6. Bode diagram of the open-loop transfer function from V_{ds} to V'_{ps} in case (ii) (K_{ref} = 1, 2, 3,4, 5)

drop at the real line section. Similarly, the feeder resistance R_{L2} is also set to 12.5 Ω. The current control time constant T_{acr} is set to 5 ms to ensure that the response is faster than the overall external feedback loop, and larger than the control calculation period.

Under the conditions listed in Table I, the Bode diagram of Fig. 3 with gain K_{ref} = 1–5 is shown in Fig. 5. The equilibrium points of the Bode diagram and the phase margin at each gain are listed in Table II. Fig. 5 and Table II show that the gain at the stability limit is K_{ref} = 4 in case (i). Similarly, a Bode diagram is described for case (ii). The Bode diagram in Fig. 4 with gain K_{ref} = 1–5 is shown in Fig. 6. The equilibrium points of the Bode diagram and the phase margin at each gain are listed in Table III. The Bode diagram exhibited the same tendency as that in Fig. 5 when the gain in the frequency band around the transition to the unstable side is considered. Focusing on this part, the stability limit gain ~~was~~ is considered as K_{ref} = 3 in case (ii).

3. Experimental verification utilizing downscaled model

The validity of the proposed gain design method in the section 2 is evaluated through an experiment utilizing downscaled model of the assumed system shown in Fig. 1.

A. Configurations of the experiment utilizing downscaled model

In this section, the results of the 1 kW class downscaled model experiments with different gains K_{ref} in models (i) and (ii) are presented. The experimental circuit configuration is shown in Fig. 7. In this experiment, a 200 V 50 Hz three-phase AC power supply is converted to 300 V DC using a transformer and diode rectifier to simulate the traction substation. The storage battery is modelled using a regenerative DC power source of 52 V. The parameters of the experimental setup are the same as those listed in Table I. The induction motor is driven by indirect field-oriented control.

B. Results of the experiment utilizing downscaled model

The value of the gain K_{ref} in the experiment is determined based on the results discussed in Section 2. In particular, for case (i), the experimental results for K_{ref} = 1 and 3 are shown in Fig. 8. For case (ii), the experimental results for K_{ref} = 2 and 4 are shown in Fig. 9. The difference between the overhead catenary line voltage and charge/discharge start voltage determines the value of the charging/discharging current. This current flows into the capacitor and determines the FC voltage of the WESS. The FC voltage of the

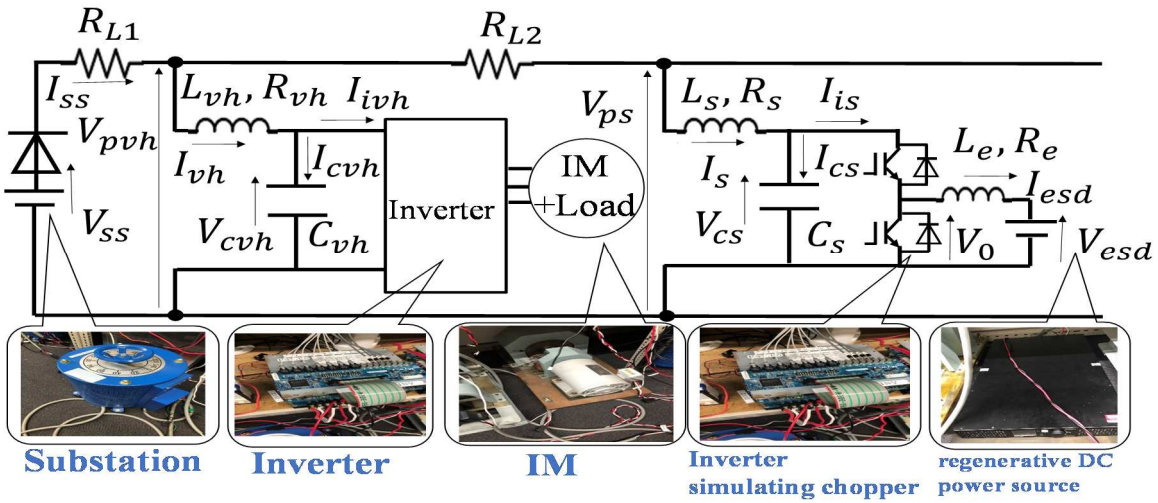

Fig. 7. Experimental circuit utilizing downscaled model

WESS, which is the output of the transfer function studied in Section 2, is used as the evaluation index in terms of stability. Fig. 6 shows that the oscillation increased as the gain K_{ref} increase, and divergence is observed at K_{ref} =3. The same tendency is observed in case (ii), where the oscillation of V_{cs} became more significant at K_{ref} = 4. Because there are parameter errors in the proposed model for the dynamic analysis in Section 2, it is necessary to design the K_{ref} by considering some phase margins. In other words, it is necessary to maintain a phase margin of about 25–30° from the unstable gain that is shown in the experimental results. Fig. 4 shows that for practical applications, it is better to design with a phase margin of +45° during discharge. Based on the same idea, it is preferable to have a phase margin of +25° during charging.

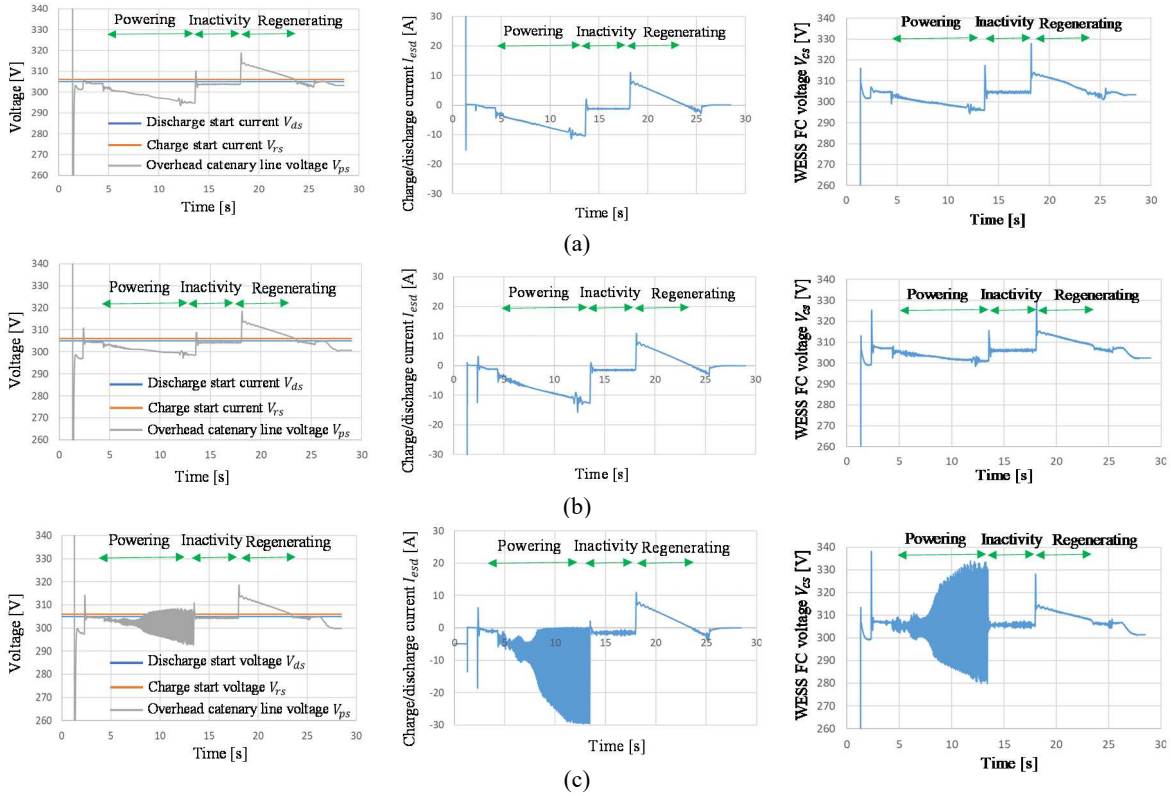

Fig. 8. Overhead catenary line voltage V_{ps}, charge/discharge current I_{esd} , and WESS FC voltage V_{cs} at each gain (a)K_{ref} =1, (b) K_{ref} =2, and (c)K_{ref} =3

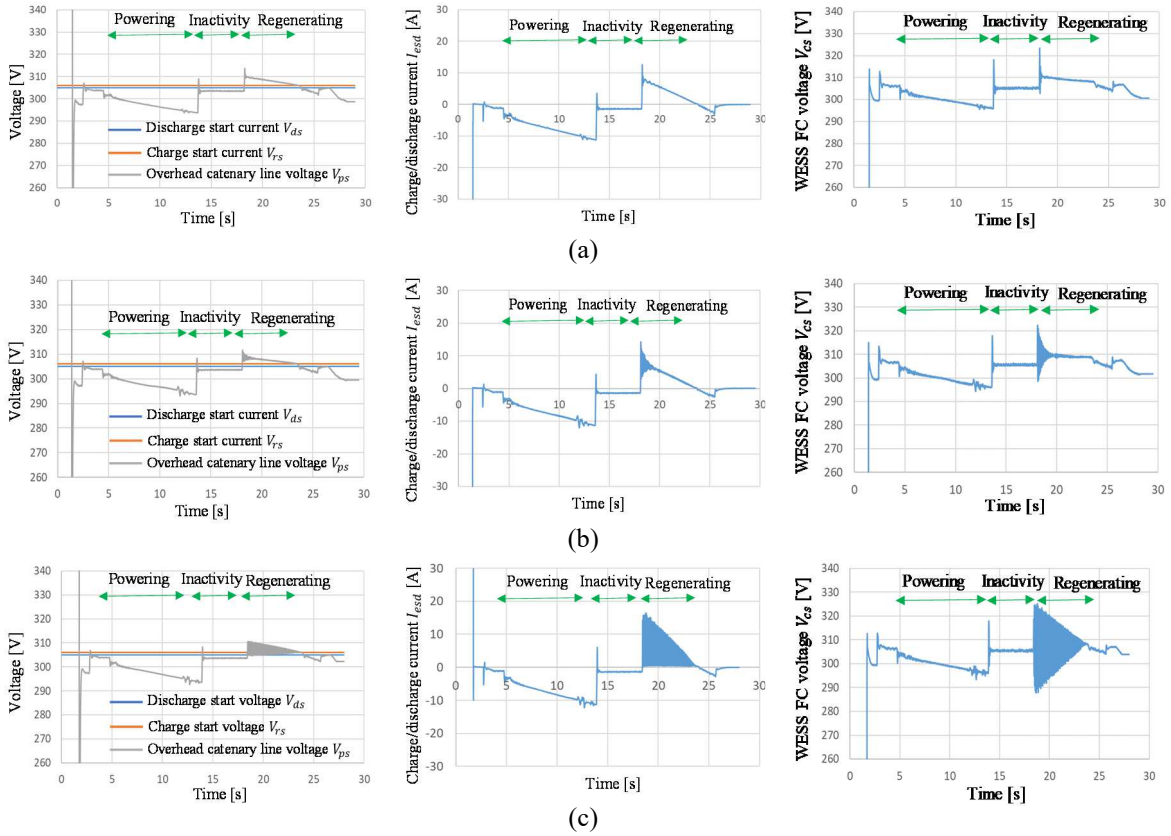

Fig. 9. Overhead catenary line voltage V_{ps}, charge/discharge current I_{esd} , and WESS FC voltage V_{cs} at each gain (a)K_{ref} =2, (b) K_{ref} =3, and (c)K_{ref} =4

4. Verification of the energy-saving effect by real-scale power feeder simulation

A. Conditions for the evaluation of the energy saving by numerical simulation

In this section, the gain is designed with a phase margin of +45° and +25° during discharging and charging, respectively, based on the results of the design in Sections 2 and 3. The parameters of the real scale system are listed in Table IV. The Bode diagram in Fig. 3 is shown in Fig. 10. The equilibrium points and the phase margin at each gain are shown in Table V. The Bode diagram for Fig. 4 is shown in Fig. 11. The equilibrium points and the phase margin at each gain are ~~is~~ shown in Table VI. The parameters are determined based on a real-scale system. The gains are determined by the proposed design method: the discharge gain K_{ref} = 23 and charge gain K_{ref} = 18. The energy-saving effect of the difference between the gain of the proposed design method and the small-gain K_{ref} is compared. The locations of the stations, substations, and the WESS are shown in Fig. 12. The train diagram is shown in Fig. 13. The train parameters are listed in Table VII.

Table IV. Real-scale parameters of the assumed system

Symbol	Parameters	Value
C_{vh}	FC capacitance of the train	37.5 mF
L_{vh}	FL inductance of the train	3.0 mH
R_{vh}	FL resistance of the train	0.1 Ω
C_s	FC capacitance of the wayside energy storage system	37.5 mF
L_s	FL inductance of the wayside energy storage system	3.0 mH
X_{L1}	Distance between the train and the wayside energy storage system	4 km
X_{L2}	Distance between the train and substation	4 km
R_s	FL resistance of the wayside energy storage system	0.1 Ω
R_{L1}	Feeder resistance between the train and the wayside energy storage system	0.142 Ω
R_{L2}	Feeder resistance between the train and substation	0.142 Ω
T_{acr}	Time constant of current control	2 ms
T_c	Time constant of low-pass filter	50 ms

B. valuation of the energy saving effect

The comparison of the energy-saving effect according to the difference between the gain K_{ref} of the proposed design method and the smaller gain K_{ref} = 10 is presented in Table VIII. K_{ref} = 10 is set as the actual conventional and conservative gain

Table V. Real-scale equilibrium points and phase margin at each gain in case(i)

(a) Equilibrium points in case (i) of the real-scale

Parameters	$K_{ref} = 10$	$K_{ref} = 23$	$K_{ref} = 50$
Chopper inflow current I_{is0} [A]	1890	1856	1834
WESS FC voltage V_{cs0}[V]	1405.5	1433.3	1451.9
Chopper lower side voltage V_{00}[V]	740.3	696.7	688.9
Discharge current I_{esd0}[A]	770.4	1040.4	1199.8

(b) Phase margin in case (i) of the real-scale

Gain value	Phase margin[deg]
10	+95
23	+45
50	+2

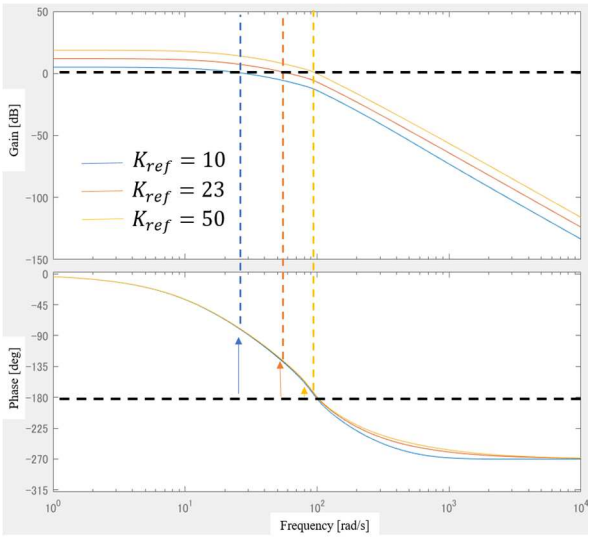

Fig. 10. Bode diagram of the open-loop transfer function from V_{ds} to V'_{ps} in case (i) of the real-scale

Table VI. Real-scale equilibrium points and phase margin at each gain in case(ii)

(a) Equilibrium points in case (ii) of the real-scale

Parameters	$K_{ref} = 10$	$K_{ref} = 18$	$K_{ref} = 50$
Chopper inflow current I_{is0} [A]	444.3	556.1	686.5
WESS FC voltage V_{cs0}[V]	1663.5	1621.6	1572.9
Chopper lower side voltage V_{00}[V]	795.3	804.9	815.1
Discharge current I_{esd0}[A]	929.4	1120.5	1324.7

(b) Phase margin in case (ii) of the real-scale

Gain value	Phase margin[deg]
10	+29
18	+25
50	-3

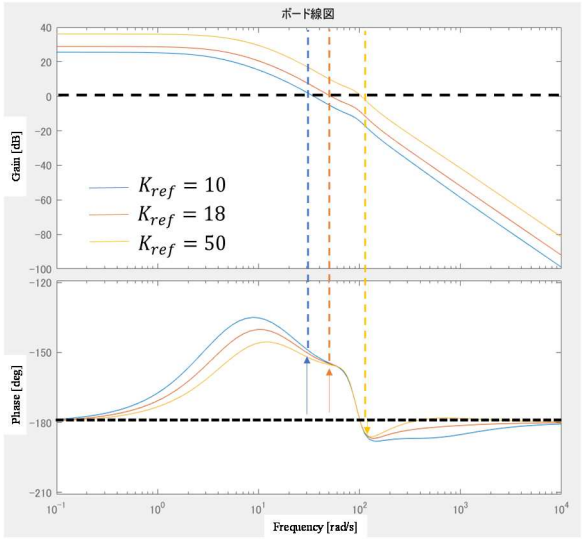

Fig. 11. Bode diagram of the open-loop transfer function from V_{ds} to V'_{ps} in case (ii) of the real-scale

value. Table VIII shows that the output energy decrease only at the substations near the WESS. There are two reasons for this result.

Table VII Simulation parameters

Parameters		Value
substation	No-load output voltage	1575 V
Train	Number of the trains	8
	Number of the motors	16
	Mass of units	306 t
	Maximum acceleration	3.5 km/h/s
	Deceleration	4.9 km/h/s
	Maximum speed	100 km/h
	Voltage to start to apply light-load regenerative brake control	1700 V
	Voltage to stop apply light-load regenerative brake control	1830 V
	SIV power consumption	10 kVA
WESS	Voltage to start to charge	1610 V
	Voltage to start to discharge	1500 V
	Power capacity of charging	1000 kW
	Power capacity of discharging	1000 kW
	Maximum input current	1330 A
	Maximum output current	1330 A
	Output voltage of the battery	748 V
Other	Feeder resistance	0.0356 Ω/km

Table VIII. Simulation results of substation energy consumption

Substation name	Discharging $K_{ref} = 23$ Charging $K_{ref} = 18$	Discharging $K_{ref} = 10$ Charging $K_{ref} = 10$
SS. A[kWh]	575.6	575.6
SS. B[kWh]	1077	1077
SS. C[kWh]	981.9	981.6
SS. D[kWh]	**1064**	**1071**
SS. E[kWh]	**1612**	**1619**
SS. F[kWh]	241.2	241.4

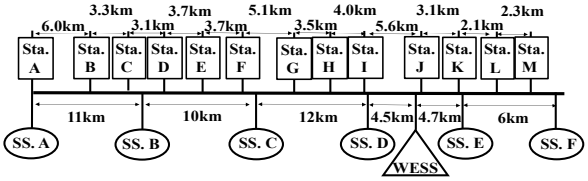

Fig. 12. Overview of simulation conditions

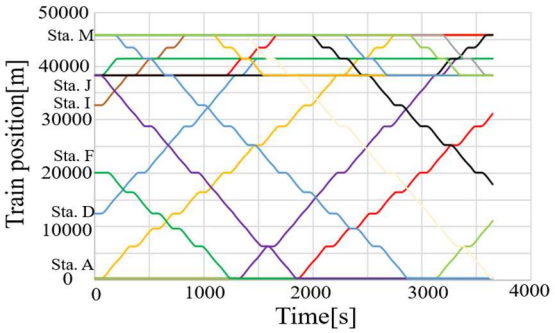

Fig. 13. Train diagram

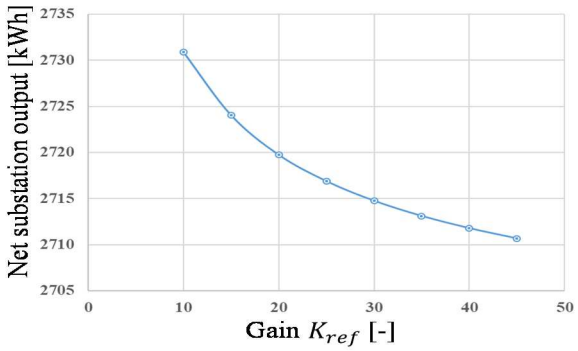

Fig. 14. Relationship between the gain K_{ref} and net output energy

1. A feeder circuit with a total length of approximately 50 km is assumed in the simulation. Therefore, the regenerative energy from the distant braking train cannot be charged to the WESS owing to the large voltage drop at the feeder resistance.

2. Because the effects of suppressing the overhead line voltage fluctuations are limited to the vicinity of the WESS, the effect of reducing the energy consumption of the powering-train is also limited to the vicinity of the WESS.

The slight increase in the output energy at substation C may be attributed to the change in power flow near the adjacent substation D as a result of the change in the output of the WESS. However, as seen in Table XII, the effect is small. For these reasons, the energy-saving effect is evaluated in substations D and E, which are located on both sides of the WESS. To make a comparison under fair conditions, the energy-saving effect is determined by calculating the net output energy from equation (11).

$$E_{\text{out}} = E_{\text{SSout}} + E_{\text{WESSout}} - E_{\text{WESSin}} \tag{11}$$

where E_{out} is the net output energy and E_{SSout} is the sum of the output energies of substations D and E in Table VIII. E_{WESSout} and E_{WESSin} are the discharge energy and charge energy of the storage device, respectively. The relationship between the net output energy calculated from equation (11) and the gain K_{ref} is shown in Fig. 14. It can be seen that the larger the gain, the higher the energy-saving effect. When $K_{\text{ref}} = 45$, and the phase margin is zero, the energy can be reduced by 0.74%. When the phase margins +45 ° and +25 °during discharging and charging, respectively, are assumed, an energy reduction of 0.37% is observed.

5. Conclusion

In this paper, a method for determining the gain K_{ref} was proposed, which was set to a conservative value by trial and error based on experience. Two feeder circuit models for the proposed design method were investigated: (i) when the train is powering and the WESS discharging; and (ii) when the train is regenerating and the WESS charging. From the Bode diagram of the open-loop transfer function of the proposed linearized models, the marginal gain K_{ref} from the perspective of stability can be obtained by

focusing on the phase margin. The results of the analysis and downscaled model experiments showed good agreement, thus confirming the validity of the proposed design method. The energy-saving effect of applying the gain of the proposed design method to a real-scale system was also considered. By applying the gains determined from the proposed design method to the real-scale system, it was observed that the substation output energy decreased by up to 0.74%. In conclusion, the proposed method enables the design of the WESS power control system that achieves the maximum energy-saving effect while maintaining stability.

References

[1] T. Koseki: “Technical Trends of Rilway Traction in the World,” IEEE IPEC, Sapporo, pp.2836-2841, (2010)

[2] H. Kobayashi, K.Kondo: “Control Method for Increasing Motor Power of DC-electrified Railway Vehicle with an Onboard Energy Storage System”, IEEJ Journal of Industry Applications,Vol.10 No.5, pp.520-527, (2021)

[3] L. Alferi, L. Battistelli, and M. Pagano: “Impact on railway infrastructure of wayside energy storage systems for regenerative braking management: a case study on a real Italian railway infrastructure,” IET Electr. Syst. Transp. Vol.9 lss.3, pp. 140–149, (2019)

[4] K. Pham, R. Eacker, M. Burnett, and M. Bardslkey, “A step forward or backward? Sound transit opts for 1500 VDC traction electrification,” in Proc. ASME/IEEE Joint Railroad Conf., Newark, NJ, USA, pp. 67–72, (2000)

[5] K. Sato, H. Kato, and T. Fukushima: “Outstanding Technical Features of Traction System in N700S Shinkansen New Generation Standardized High Speed Train”, IEEJ Journal of Industry Applications, Vol. 10 No.4, pp.402-410, (2021)

[6] K. Sato, H. Kato, and T. Fukushima: “Development of SiC Applied Traction System for Next-Generation Shinkansen High-Speed Trains”, IEEJ Journal of Industry Applications, Vol. 9 No.4, pp.453-459, (2020)

[7] K. Tesaki, Y. Ishida, and M. Hagiwara: “Control and Experimental Verification of a Bidirectional Non-isolated DC-DC Converter Based on Three-level Flying-Capacitor Converters”, IEEJ Journal of Industry Applications, Vol.10 No1, pp.114-123, (2021)

[8] H. Kobayashi, J. Asano, T. Saito, K. Kondo:“A Power Control method to Save Energy for Wayside Energy Storage Systems in DC-electrified Railway System”, Electrical engineering in Japan, 2016-07, Vol.196, p.56-66.

[9] T. Funaki, N. Kimura, K. Matsu-ura:“Suppression of DC Line Current Oscillation of HV DC Transmission System Using Voltage Source Forced Commutation Converter”, Electrical engineering in Japan, 1994, Vol.114, p.123-132

[10] A. Emadi, A. Khaligh, Claudio H. Rivetta, Geoffrey A. Williamson:”Constant power loads and negative impedance instability in automotive systems: definition, modeling, stability, and control of power electronic converters and motor drives”, IEEE Transactions on Vehicular Technology, Vol.55, Issue 4, pp.1112-1125, (2006)

[11] Xuan Z, Lie X, Yongdong L, Zedong Z, Kui W: “Stabilization and assessment of interaction dynamics for More Electric Aircraft”, Proceedings on the IEEE 8th International Power Electronics and Motion Control Conference (IPEMC-ECCE Asia) , DOI 10.1109/IPEMC.2016.7512401, 2016